RSC Advances

PAPER

View Article Online
View Journal | View Issue

Cite this: *RSC Adv.*, 2018, **8**, 37774

A facile synthesis methodology for preparation of Ag–Ni-reduced graphene oxide: a magnetically separable versatile nanocatalyst for multiple organic reactions and density functional study of its electronic structures†

Madhurya Chandel, Priyanka Makkar, Barun Kumar Ghosh, Debabrata Moitra and Narendra Nath Ghosh *

Here, we report a simple *'in situ'* co-precipitation reduction synthesis method for the preparation of nanocatalysts composed of Ag, Ni nanoparticles, and reduced graphene oxide (RGO). First-principles calculations based on Density Functional Theory (DFT) were performed to obtain the electronic structures and properties of Ag–Ni-graphene superlattice and to understand the interfacial interactions which exist at the interface between Ag, Ni, and graphene. The catalytic performance of the synthesized catalysts $(Ag_xNi_{(1-x)})_yRGO_{(100-y)}$ were evaluated for four reactions (i) reduction of 4-nitrophenol (4-NP) in the presence of excess $NaBH_4$ in aqueous medium, (ii) A3 coupling reaction for the synthesis of propargylamines, (iii) epoxidation of styrene, and (iv) 'Click reaction' for the synthesis of 1,2,3-triazole derivatives. For all of these reactions the catalyst composed of Ag, Ni, and RGO, exhibited significantly higher catalytic activity than that of pure Ag, Ni, and RGO. Moreover, an easy magnetic recovery of this catalyst from the reaction mixture after completion of the catalytic reactions and the good reusability of the recovered catalyst is also reported here. To the best of our knowledge, this is the first time the demonstration of the versatile catalytic activity of $(Ag_xNi_{(1-x)})_yRGO_{(100-y)}$ towards multiple reactions, and the DFT study of its electronic structure have been reported.

Received 5th October 2018
Accepted 4th November 2018

DOI: 10.1039/c8ra08235a

rsc.li/rsc-advances

1. Introduction

For the last couple of decades, the applications of graphene and graphene-based materials have been explored extensively in myriad fields including electronics, sensors, solar cells, structural materials, catalysis, microwave absorbing materials, supercapacitors, *etc.*[1–5] Graphene has proved its capability to become a material of paramount importance by exhibiting several excellent properties (such as, electrical conductivity, mechanical strength, chemical stability, lightweight, *etc.*).[1,2,6,7] Several researchers have reported the application of graphene or Reduced Graphene Oxide (RGO) as the support to construct heterogeneous catalysts, where catalytically active sites are immobilized on the surface of graphene or RGO sheets.[6–11] However, to the best of our knowledge, to date, the development of graphene-based catalysts, which can exhibit versatile high catalytic activity towards multiple organic reactions as well as easy magnetic recovery from reaction mixtures, is limited.[10,12]

To develop an efficient, but versatile and magnetically separable catalyst, we have synthesized the catalysts which are composed of varying amounts of Ag, Ni nanoparticles, and RGO. We have investigated the catalytic activity of the synthesized catalysts towards four important reactions: (i) reduction of 4-nitrophenol (4-NP) in the presence of $NaBH_4$, (ii) A3 coupling reaction for the synthesis of propargylamines, (iii) epoxidation of styrene, and (iv) 'Click reaction' for the synthesis of 1,2,3-triazole derivatives in aqueous medium. We have chosen to develop a versatile catalyst for these reactions because of the following reasons:

(i) Reduction of 4-nitrophenol (4-NP) to 4-aminophenol (4-AP): nitrophenols and their derivatives are widely used, or produced in many industries, such as dye-based industries, textiles, leather, pesticides, pharmaceuticals, iron and steel manufacturing, foundries, refinery, *etc.*[8,11,13] Effluents of these industries contain a significant amount of 4-NP and other nitrophenols. These effluents, when coming in contact with natural water bodies, cause water pollution, because these nitrophenols are harmful to the kidney, liver, central nervous systems, *etc.*[11,14,15] Therefore, to address this environmental

Nano-materials Lab, Department of Chemistry, Birla Institute of Technology and Science, Pilani K. K. Birla Goa Campus, Goa-403726, India. E-mail: naren70@yahoo.com; Fax: +91 832 2557033; Tel: +91 832 2580318

† Electronic supplementary information (ESI) available. See DOI: 10.1039/c8ra08235a

pollution issue removal or destruction of 4-NP (or similar nitrophenols) from the polluted aquatic system is very crucial. On the other hand, reduction of 4-NP produces 4-AP, which is an important chemical for many pharmaceutical industries for the production of antipyretic and analgesic drugs, *etc.*[10,11,14,16] Moreover, several researchers have investigated the reduction of 4-NP to 4-AP as a model reaction to evaluate the catalytic activity of variety of nanostructured catalysts because this reaction is easy to perform, convincing, and trustworthy for this purpose.[8,9,11,13,14,16]

(ii) A3 coupling reaction: this reaction can be used to synthesize propargylamines through a one-pot reaction using the combination of three starting materials (*e.g.* aldehyde, amine, and alkyne). Propargylamines are an important class of compound for the preparation of several biologically active nitrogen compounds, and also crucial intermediates for many pharmaceuticals and natural products.[17,18] Traditional methods for propargylamines synthesis (such as the nucleophilic addition of Grignard reagents or lithium acetylide to imines, *etc.*) involve multistep synthesis or purification.[19–21] Use of moisture sensitive reagents in a regulated reaction condition is one of the limitations associated with these traditional methods which limits the large-scale reaction.[18,21] To avoid these problems, the coupling of aldehydes, amines, and alkynes *via* A3 coupling reaction over the heterogeneous catalysts has emerged as a promising approach to synthesize propargylamines.[17,18,22,23]

(iii) Epoxidation of styrene: epoxidation is an important reaction for the chemical industries because of the wide range applications of epoxy resins, including synthesis of many commodities, useful intermediates for the synthesis of many pharmaceutical products, and fine chemicals.[24,25] Conventional methodologies for the epoxidation of styrene (such as the non-catalytic process using chlorine, co-epoxidation process, organic peroxide and peracid-based catalytic process, *etc.*) suffer from some disadvantages, such as the production of the large amount of undesirable by-products, harsh reaction conditions, cost-effectiveness, separation problem associated with homogeneous catalysts, *etc.*[10,26,27] Therefore, till date, several researchers are engaged in developing novel catalysts for chlorine-free epoxidation reaction.[27–30]

(iv) Click reaction: synthesis of triazoles by 'Click reaction' has gained immense attention due to the use of triazoles as biologically active chemicals, agrochemicals, pharmaceuticals, drug molecules with significant anti-HIV activity, antimicrobial activity against Gram-positive bacteria, *etc.*[31–34] Several researchers have developed various types of heterogeneous catalysts for the synthesis of triazole derivatives.[23,32,34,35] However, in some cases the limitations associated with these procedures are the requirement of elevated reaction temperature, the formation of undesired products, low yields, use of homogeneous catalysts which are difficult to separate from products, *etc.*[31,35,36]

Though several nanostructured catalysts exhibit high catalytic activity due to their high surface area, their tendency to form agglomerates and difficulty in separation by easy filtration process are major limitations for large-scale applications. To overcome these limitations immobilization of nanocatalysts on high surface area support and developing magnetically separable catalyst are attractive strategies.[10,14,18,34,37,38] Therefore, to develop a catalyst which will exhibit catalytic activity towards all of the above mentioned organic reactions along with easy magnetic separation, we have designed the catalyst where Ag and Ni nanoparticles are intimately coexisting, and these nanoparticles are immobilized on the surface of nanometer thin sheets of RGO. The reasons for choosing Ni and Ag nanoparticles as catalytically active components of this catalyst is that Ni and Ag nanoparticles can participate in these reactions by stabilizing intermediates through the formation of coordination complexes and thus help the reactions to proceed forward.[22,23,39–41] Moreover, as Ni nanoparticles are magnetic in nature, the presence of Ni introduces a magnetic character in the catalyst and makes the catalyst magnetically separable. RGO provides a high surface area, which helps the reactant molecules to get adsorbed on the surface of the catalyst and to come in contact with catalytically active sites (here Ag and Ni). It is also expected that the high conducting nature of RGO will help in the electron transfer process of these catalysis reactions.[1,3,6]

Herein, we are reporting an '*in situ*' co-precipitation reduction technique for the preparation of a versatile catalyst, $((Ag_x\text{-}Ni_{(1-x)})_yRGO_{(100-y)})$, for (i) reduction reaction of 4-nitrophenol (4-NP) in presence of $NaBH_4$, (ii) A3 coupling reaction for the synthesis of propargylamines, (iii) epoxidation reaction of styrene, and (iv) 'Click reaction' for the synthesis of 1,2,3-triazole derivatives in aqueous medium and magnetic recovery and reusability of the catalyst. We have also performed the first-principles calculations based on Density Functional Theory (DFT) to understand how the interfacial interactions between Ag, Ni, and RGO influence their electronic structures, due to which the synergistic effect originates and the synthesized catalyst exhibits superior catalytic activity. To the best of our knowledge, this is the first time the catalyst, containing Ag, Ni nanoparticles and RGO, has been reported which can exhibit catalytic property for these four reactions.

2. Experimental

2.1. Materials

Acetone, hydrazine hydrated ($N_2H_4 \cdot H_2O$), polyvinylpyrrolidone (PVP), sodium hydroxide (NaOH), sodium nitrate, sulphuric acid (H_2SO_4), hydrochloric acid (HCl), sodium nitrate ($NaNO_3$), 4-nitrophenol (4-NP), and nickel(II)nitrate hexahydrate ($Ni(NO_3)_2 \cdot 6H_2O$) were purchased from Fischer Scientific. Silver nitrate ($AgNO_3$), potassium permanganate ($KMnO_4$), sodium azide (NaN_3), 30% H_2O_2 solution, ethylene glycol, acetonitrile, methanol, dichloromethane, toluene, chloroform, diethylamine, and aniline were purchased from Merck, India. Sodium borohydride ($NaBH_4$), aldehydes, piperidine, phenylacetylene, styrene, styrene oxide, cyclohexene oxide, epichlorohydrin, *tert*-butyl hydroperoxide (TBHP in 5–6 M decane), and graphite powder (mean particle size of <20 mm) were purchased from Sigma-Aldrich. All the chemicals were used without further purification. Distilled water was used throughout the experiment.

2.2. Synthesis of $((Ag_xNi_{(1-x)})_yRGO_{(100-y)})$

We have synthesized the nanocatalysts composed of the different amount of Ag nanoparticle, Ni nanoparticle, and RGO, in two steps. In the first step, graphene oxide (GO) was prepared by using the modified Hummers method (method of GO synthesis is provided in ESI†).[42] In the next step, a mixture of ethylene glycol (EG) and PVP (molar ratio 2 : 1) was prepared, and the calculated amount of GO sheets were dispersed in this mixture. In this dispersion $AgNO_3$ and $Ni(NO_3)\cdot 6H_2O$ were added according to the compositions of the nanocatalyst (*i.e.* $(Ag_xNi_{(1-x)})_yRGO_{(100-y)}$, where $x = 0$–1, and $y = 0$–100). After the addition of metal nitrate salts, the mixture was stirred until the metal salts were dissolved. In this mixture, NaOH pellets were added with stirring till the pH of the mixture became ~10, and then N_2H_4 was added dropwise keeping the metal ion: N_2H_4 molar ratio 1 : 40. After complete addition of N_2H_4, this reaction mixture was refluxed at 85 °C for 15 min and then cooled to room temperature. The precipitate thus formed was magnetically separated from the reaction mixture by using a magnet externally. The collected precipitate was washed with distilled water until the pH of the washing reached ~7. Finally, the precipitate was washed with acetone and dried at 60 °C for 10 h. As a representative, the detail of the synthesis procedure for $(Ag_{0.27}Ni_{0.73})_{37}RGO_{63}$ preparation has been described in ESI.† To perform the control experiments, we have also prepared pure Ag, and pure Ni nanoparticles using the aforesaid method, without adding RGO. Pure RGO was also synthesized by reducing GO with N_2H_4. Several compositions of catalysts, containing only Ag and Ni nanoparticles (*i.e.* $Ag_xNi_{(1-x)}$), were also prepared using the same method. The code of the catalysts and the corresponding compositions are listed in Table S1 (ESI†).

2.3. Catalytic activity tests

2.3.1 Reduction of 4-nitrophenol to 4-aminophenol. To investigate the catalytic activity of the synthesized catalysts the reduction of 4-nitrophenol (4-NP) to 4-aminophenol (4-AP) was performed in the presence of excess $NaBH_4$ in an aqueous medium. The reaction was carried out in the presence of catalysts $(Ag_xNi_{(1-x)})_yRGO_{(100-y)}$ with different compositions. In a typical run, 4.5 ml of 9 mM aqueous solution of 4-NP was mixed with 1.5 ml H_2O and 1 ml of 0.2 M $NaBH_4$ solution. To this solution, 1 ml of an aqueous suspension of the catalyst (0.1 g l^{-1}) was added. 4 ml of this reaction mixture was transferred immediately in a quartz cuvette and the absorbance spectra of the solution were recorded using a UV-Vis spectrophotometer (V-570, Jasco, Japan) at an interval of 1 min. Before the addition of $NaBH_4$, the aqueous solution of 4-NP exhibited the maximum absorption (λ_{max}) at 317 nm. When the aqueous solution of $NaBH_4$ was added to the solution of 4-NP, the color of the solution became dark yellow due to the formation of phenolate ion and λ_{max} peak was red-shifted to 400 nm.[3,14] After addition of the catalyst, the color of the reaction mixture started to fade with the progress of time. The progress of the reduction of 4-NP was determined by monitoring the gradual decrease of the intensity of the λ_{max} peak (at 400 nm) with time. In this reaction, the initial concentration of $NaBH_4$ was very high, and it remained almost constant throughout the reaction. It is a well-established fact that the metal nanoparticle catalyzed reduction reaction of 4-NP in the presence of excess $NaBH_4$ proceeds *via* pseudo first-order kinetics.[3,11,14,33] As the absorbance of 4-NP is proportional to its concentration, the ratio of the absorbance of 4-NP A_t (measured at time t) to A_o (at $t = 0$) is equal to C_t/C_o (where C_o is the initial concentration and C_t is the concentration at time t of 4-NP). The apparent rate constant (k_{app}) was determined using the following equations:[3,14]

$$dC_t/d_t = -k_{app}C_t \quad (1)$$

$$\ln(C_t/C_o) = \ln(A_t/A_o) = -k_{app}\, t \quad (2)$$

The value of k_{app} was calculated from the slope of the $\ln(A_t/A_o)$ *vs.* time plot.

2.3.2 Synthesis of propargylamines by A3 reaction. The catalytic activity of the synthesized catalyst $(Ag_xNi_{(1-x)})_y$-$RGO_{(100-y)}$ was tested for the synthesis of propargylamine *via* an A3 coupling reaction. In a typical reaction, in a 25 ml round bottomed flask 2 mmol aldehyde, 2.4 mmol amine, 3 mmol phenylacetylene, and 50 mg catalyst were mixed with 10 ml acetonitrile under the nitrogen atmosphere. Then, the reaction mixture was stirred for 12 h at 100 °C. The progress of the reaction was monitored by Thin Layer Chromatography (TLC). After completion of the reaction, the reaction mixture was allowed to cool down, and from the reaction mixture catalyst was recovered magnetically. The solvent was removed using a rotavapor and the collected crude product was purified using a gel column chromatography with petroleum ether and ethyl acetate (10 : 2) as eluent. The catalysis reaction was performed at different reaction conditions and it was observed that the highest yield was obtained when the reaction temperature was 100 °C, reaction time was 12 h and acetonitrile as the solvent. After optimizing the reaction conditions, the A3 coupling reaction was also performed by using different types of aldehydes and amines to demonstrate the effectiveness of the synthesized catalyst.

2.3.3 Epoxidation of styrene. The catalytic activity of the synthesized $(Ag_xNi_{(1-x)})_yRGO_{(100-y)}$ catalyst was tested towards the epoxidation of styrene using TBHP as an oxidizing agent. In a typical experiment, 5 mmol styrene, 4 ml acetonitrile, and 25 mg catalyst were mixed in a round bottomed flask, and the mixture was sonicated for 5 min. In this mixture, 12.5 mmol of TBHP was added and then the reaction mixture was refluxed under the nitrogen atmosphere at 100 °C. The progress of the reaction with time was monitored by drawing 0.1 ml aliquot from the reaction mixture and the catalyst was separated from the reaction mixture using a magnet externally. Then the reaction mixture was analyzed using a gas chromatograph (GC). The conversion and product selectivity were calculated using the following eqn (3) and (4) respectively:[10,15]

$$\text{Conversion } (\%) = \frac{\text{moles of reactant converted}}{\text{moles of reactant feed}} \times 100 \quad (3)$$

$$\text{Product selectivity (\%)} = \frac{\text{moles of product formed}}{\text{moles of reactant converted}} \times 100 \quad (4)$$

The reaction was conducted under different reaction conditions. It was observed that the highest amount of styrene conversion was achieved when the reaction was performed at 100 °C for 10 h with 1 : 2 styrene : TBHP ratio. Therefore, this reaction condition was used when the reaction was performed with the catalysts having different compositions.

2.3.4 Synthesis of 1,4-disubstituted 1,2,3-triazoles by 'Click reaction'. For the synthesis of 1,4-disubstituted 1,2,3-triazoles by 'Click reaction', the synthesized materials $(Ag_xNi_{(1-x)})_y$-$RGO_{(100-y)}$ were used as catalyst. Here, 2-phenyl-2-(4-phenyl-1*H*-1,2,3-triazol-1-yl) ethanol was synthesized in aqueous medium as a model reaction. In a typical synthesis, 1 mmol styrene oxide, 1.5 mmol sodium azide, 1 mmol phenylacetylene, and 25 mg of $(Ag_xNi_{(1-x)})_yRGO_{(100-y)}$ were mixed with 3 ml water in a round bottomed flask. This reaction mixture was refluxed at 100 °C for 12 h with constant stirring. Then the reaction mixture was allowed to cool down to room temperature, and the catalyst was separated magnetically. The product was separated from the reaction mixture by filtration, followed by recrystallization. To determine the optimized catalyst composition, the reactions were performed using the catalysts having different amounts of Ag, Ni, and RGO. As $(Ag_{0.27}Ni_{0.73})_{37}RGO_{63}$ was found to be the most effective catalyst, the Click reaction was also carried out using different types of epoxy with this as catalyst.

2.3.5 Magnetic recovery of the catalyst and recycling. After each reaction cycle, the catalyst was separated from the reaction mixture by applying an external permanent magnet (N35 grade NdFeB magnet having energy product $BH_{max} = 33$–36 MGO) and then the catalyst washed with distilled water and ethanol. It was observed that no unreacted molecule was remained adsorbed in the catalyst. After washing, the catalyst was dried at 100 °C for 8 h in an oven, and then used for the next reaction cycle.

2.4. Characterization

The synthesized pure Ni, pure Ag, $Ag_xNi_{(1-x)}$, and $(Ag_xNi_{(1-x)})_y$-$RGO_{(100-y)}$ catalysts were characterized by X-ray diffraction (XRD), thermogravimetric analysis (TGA), Fourier Transform Infrared spectra (FT-IR), Raman, Field Emission Scanning Electron Microscope (FESEM), energy dispersive X-ray analysis (EDX), and Vibrating Sample Magnetometer (VSM). The products which were obtained from catalysis reactions were characterized by Liquid Chromatography-Mass Spectrometer (LC-MS), Proton Nuclear Magnetic Resonance (^{1}H NMR), Gas Chromatography (GC), and Differential Scanning Calorimetric (DSC) (details of the characterization are discussed in ESI†).

2.5. First-principles calculations

We have performed the first-principles quantum mechanical calculations based on DFT to obtain the electronic structures of Ni, Ag, Ag–Ni interface, and Ag–Ni-graphene superlattice. Here, we have used Quantum ESPRESSO computational package[43] to calculate the ground state structures, binding energy, Density of States (DOS), and Projected Density of states (PDOS) using a plane wave set and pseudopotentials. DFT was used with Generalized Gradient Approximation (GGA)[44] and parameterized by Perdew, Burke, and Ernzerhof (PBE).[45] Kohn–Sham orbitals were expanded in a plane-wave basis set up to the kinetic energy cutoff 25 Ry (340 eV). The convergence criterion for the self-consistence calculation was 10^{-7} Ry per Bohr (0.0257 eV Å^{-1}). For calculating the final electronic properties of the structures, and empirical dispersion-corrected density functional theory (DFT-D2) approach, which was proposed by Grimme[46,47] was employed. To account for the intermolecular interactions and van der Waals (vdW) interactions, the Grimme-D2 correction was used.[12]

In the present study five systems were investigated (i) superlattice of pure Ag with face-centered cubic structure (space group $Fm\bar{3}m$), (ii) pure Ni with face-centered cubic structure (space group $Fm\bar{3}m$), (iii) graphene superlattice, (iv) Ag–Ni interface, and (v) Ag–Ni-graphene superlattice. Ultrasoft pseudopotential for these systems were constructed by using 17, 16, and 4 electrons for Ag ($4p^64d^{10}5s^1$), Ni ($3p^63d^84s^2$), and C ($2s^22p^2$), respectively. From the Quantum ESPRESSO website, the pseudopotentials of Ag, Ni, and C were chosen.[48] To select the *k*-points mesh, the Monkhorst–Pack approach was used[49] and the details of *k* points for each system are provided in the computational details section in the ESI.† The Brillouin zone integration of these systems was performed with Methfessel–Paxton smearing technique[50] for Ag (111) slab, and Ni (111) slab, Marzari–Vanderbilt smearing technique[51] for graphene, Ag–Ni interface, and Ag–Ni-graphene superlattice. Here, the smearing parameter was 0.005 Ry. The Binding energy of Ag–Ni-graphene superlattice was calculated from the difference between the total energy of the Ag–Ni-graphene superlattice and the sum of each system alone (Ag–Ni interface and graphene). The sizes of the unit cells of the simulated systems are listed in Table S2 (ESI†). The details of the sample input files for the geometric optimization of Ag, Ni, graphene, Ag–Ni, and Ag–Ni-graphene superlattice are provided in the computational details section in ESI.†

3. Results and discussion

3.1. Structure and morphology of the synthesized $(Ag_xNi_{(1-x)})_yRGO_{(100-y)}$ catalyst

The room temperature wide-angle XRD was used to identify the crystalline phases which were present in the synthesized catalysts. As a representative, XRD patterns of GO, pure Ag, pure Ni, $Ag_{0.50}Ni_{0.50}$, $Ni_{30}RGO_{70}$, and $(Ag_{0.27}Ni_{0.73})_{37}RGO_{63}$ are shown in Fig. 1. The XRD patterns of other compositions of the catalysts are shown in Fig. S1–S2 (ESI†). In case of pure Ag nanoparticles, diffraction peaks at $2\theta = 38.2°$, $44.3°$, $64.6°$, and $77.3°$, which correspond to the (111), (200), (220), and (222) planes of FCC phase of Ag (ICDD no. 04–0783), were observed. XRD pattern of pure Ni sample showed the peaks at $2\theta = 44.3°$, $51.7°$ and $76.4°$ corresponding to (111), (200), and (220) planes of FCC phase of Ni (ICDD no. 04–0850). In the XRD patterns of the $Ag_xNi_{(1-x)}$ catalysts, the characteristic diffraction peaks of the only Ag and

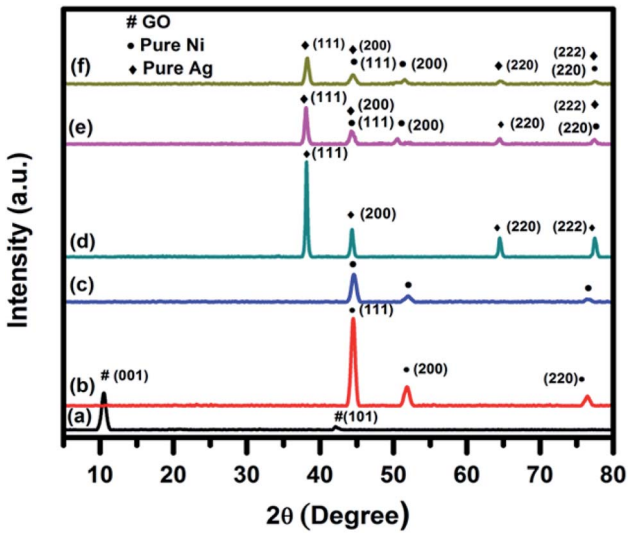

Fig. 1 Room temperature wide angle powder XRD pattern of (a) GO, (b) pure Ni, (c) $Ni_{30}RGO_{70}$, (d) pure Ag, (e) $Ag_{0.50}Ni_{0.50}$, and (f) $(Ag_{0.27}Ni_{0.73})_{37}RGO_{63}$.

Ni were present (Fig. S1, ESI†). In case of pure GO sample, an intense peak at $2\theta = 9.76^\circ$ and a small peak at $2\theta = 42.14^\circ$ were observed which represented the (001) and (101) planes of GO, respectively.[3,4,10] In the XRD pattern of $(Ag_xNi_{(1-x)})_yRGO_{(100-y)}$ samples, all the peaks which are characteristic diffraction peaks of Ag and Ni were present indicating the presence of pure Ni and Ag nanoparticles in these samples (Fig. S2, ESI†). The crystallite size of Ag and Ni particle was calculated by Scherrer's equation using the diffraction peak corresponding to (111) plane of Ag and (111) plane of Ni. The crystallite sizes of Ni and Ag nanoparticles were ~11 nm and ~15 nm, respectively. It was also observed that in the XRD patterns of $(Ag_xNi_{(1-x)})_yRGO_{(100-y)}$ samples no diffraction peaks of GO were present. Therefore, it was concluded that during the synthesis of these nanocatalysts by the '*in situ*' co-precipitation reduction technique GO was converted to RGO. TGA, FT-IR, and Raman spectroscopy of these samples also indicated this conversion of GO to RGO.

TGA and DTA of the synthesized catalysts were performed to understand the effect of temperature on the catalysts and also to determine the amount of RGO present in the catalyst (Fig. 2). In the TGA-DTA thermogram of pure GO following points were observed (i) ~11% weight loss occurred in the temperature range of 30–110 °C, which might be due to the loss of surface adsorbed water, (ii) in the temperature range of 110–290 °C, ~31% weight loss in TGA and a sharp exothermic peak at 240 °C in DTA indicated the removal of oxygen-containing functional groups (*e.g.* epoxy, carbonyl, carboxylic group) from GO in this temperature range, (iii) the complete decomposition of GO occurred in the temperature range of 300–625 °C. The exothermic nature of this decomposition was indicated by the presence of an exothermic peak at 460 °C in the DTA. The TGA thermogram of pure RGO showed (i) ~5% weight loss in 30–110 °C temperature range due to the removal of adsorbed water, and (ii) a continuous weight loss till the complete decomposition of RGO in the temperature range of 110–625 °C. DTA of RGO also showed an exothermic peak at 500 °C. From TGA-DTA thermograms of the synthesized catalysts two major points were observed (i) similar to GO and RGO, the loss of surface adsorbed water (~5 wt%) occurred in the temperature range of 30–110 °C, (ii) in the temperature range of 110–550 °C, the continuous weight loss due to the decomposition of RGO from the catalyst. This major weight loss step is similar to pure RGO. Here, the important points were noted (i) for the $(Ag_xNi_{(1-x)})_yRGO_{(100-y)}$ samples, no distinguishable weight loss step in the temperature range of 110–290 °C was observed, which was noticed in case of pure GO. This fact indicated that $(Ag_xNi_{(1-x)})_yRGO_{(100-y)}$ samples contain only a few numbers of oxygen-containing functional groups, and GO was converted to RGO *via* the partial reduction of these groups during the synthesis of the catalysts. (ii) the decomposition of RGO occurred in the catalysts at a relatively lower temperature (~550 °C) than that RGO (~625 °C). This could be due to the presence of Ag and Ni particles in the catalyst, which facilitated the decomposition of carbon, (iii) in case of the catalysts ($(Ag_xNi_{(1-x)})_yRGO_{(100-y)}$), after complete decomposition of RGO, the remaining amount of the undecomposed catalyst matched well with the expected

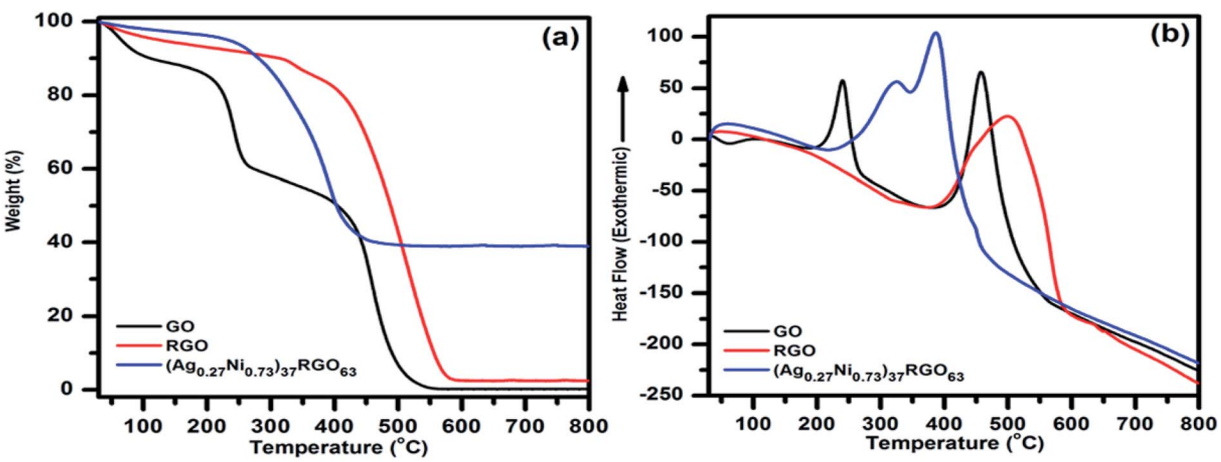

Fig. 2 (a) TGA and (b) DTA curve of GO, RGO, and $(Ag_{0.27}Ni_{0.73})_{37}RGO_{63}$.

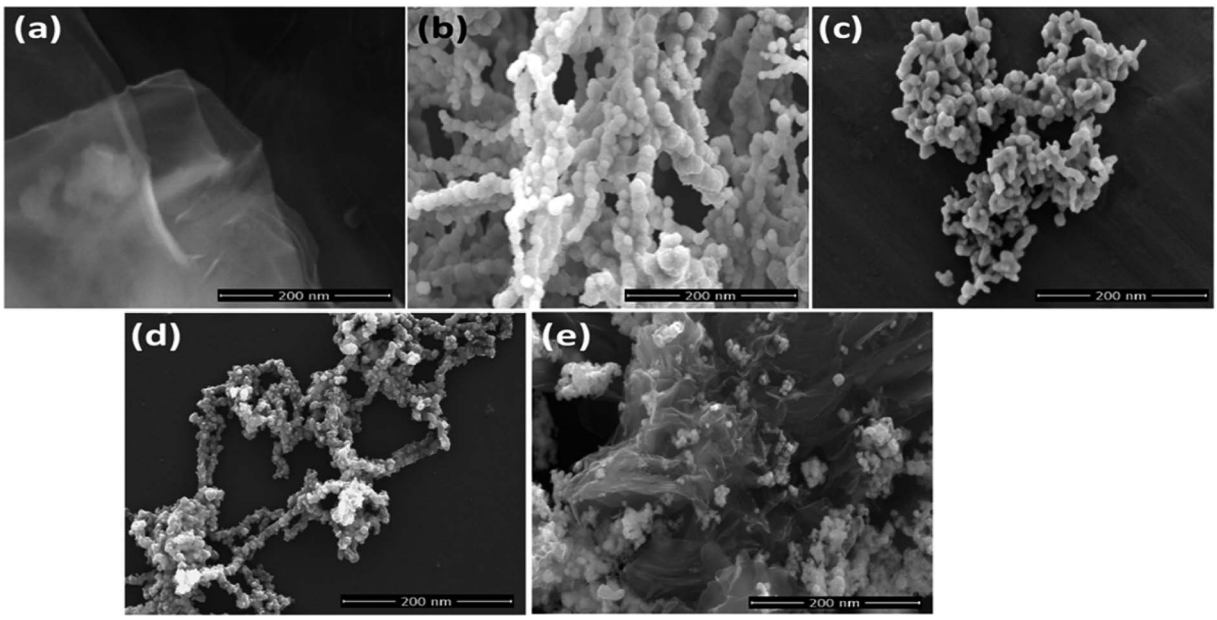

Fig. 3 FESEM images of (a) pure RGO, (b) pure Ni, (c) pure Ag, (d) $Ag_{0.50}Ni_{0.50}$, (e) $(Ag_{0.27}Ni_{0.73})_{37}RGO_{63}$.

amount of Ag and Ni in the catalyst. This is an indication that, the '*in situ*' co-precipitation reduction method, which we have adopted to prepare the catalysts, is capable of producing nanocatalysts with the desired composition of Ag, Ni, and RGO.

The FT-IR spectra of GO, pure RGO, and the catalyst $(Ag_{0.27}Ni_{0.73})_{37}RGO_{63}$ are shown in Fig. S3 (ESI†). In case of GO the peaks at (i) 1384 cm^{-1} for the C–O stretching vibration of $-CO_2H$ group, (ii) 1234 cm^{-1} for the C–O stretching vibration of an epoxy group, (iii) 1053 cm^{-1} for C–O stretching vibration were observed, which indicated the presence of carboxyl, epoxy, and carbonyl groups on the surface of GO sheets.[3,52] Moreover, the peak at 1620 cm^{-1} represented the contribution of the C=C skeletal vibration of the graphitic domain of GO.[3,52] In the FT-IR spectra of RGO and the catalyst, the disappearance of the peaks at 1730 and 1234 cm^{-1}, and decrease in the intensity of the peak at 1053 cm^{-1} indicated the reduction of the functional groups of GO during the preparation of RGO and the catalysts. It was also noted that the band at 1620 cm^{-1} (in GO sample) has been red shifted to 1545 cm^{-1} (for RGO) and 1580 cm^{-1} (for catalyst). The red shifting of this band, which corresponds to the C=C skeletal vibration, can be interpreted as the partial restoration of π–π conjugation of graphene sheet in the pure RGO as well as the catalyst.[3,52] These results clearly indicated the formation of RGO from GO during the synthesis of the catalysts.

Fig. S4 (ESI†) presents the Raman spectra of the pure GO, pure RGO, and $(Ag_{0.27}Ni_{0.73})_{37}RGO_{63}$ catalyst. In case of GO, two characteristic peaks at 1337 and 1589 cm^{-1} were observed which correspond to the D and G bands, respectively. In the case of RGO, these bands were shifted to 1328 and 1580 cm^{-1}. Raman spectra of the catalyst showed the further shifting of these D and G bands to the lower wave numbers *i.e.* at 1315 and 1563 cm^{-1}, respectively. The shifting of the Raman shift values of D and G bands to the lower bands could be attributed to the formation of RGO in the catalyst due to the reduction of GO.[4,10] The I_D/I_G ratio of GO, RGO, and the catalyst were 0.98, 1.02, and 1.15, respectively. This increase of I_D/I_G for RGO and the catalyst compared to GO might be due to the decrease in the average size of sp^2 domains upon the reduction of GO during the formation of the catalyst.[4,10]

FESEM micrographs of the synthesized pure RGO, Ag nanoparticles, Ni nanoparticle, $Ag_{0.50}Ni_{0.50}$, and $(Ag_{0.27}Ni_{0.73})_{37}RGO_{63}$ nanocomposite are shown in Fig. 3. Nanometer thin sheets were clearly visible in the micrograph of RGO. The micrographs of pure Ni and Ag showed that in both the cases almost spherical nanoparticles, having the particle size of 30–50 nm range were attached closely to each other. In case of $Ag_{0.50}Ni_{0.50}$ sample, Ag and Ni nanoparticles were randomly attached to each other. However, the large agglomerations of only Ni or only Ag particles were not observed. The micrograph of $(Ag_{0.27}Ni_{0.73})_{37}RGO_{63}$ revealed that closely attached Ag and Ni particles were immobilized on the surface of RGO sheets. Color mapping of $Ag_{0.50}Ni_{0.50}$ and $(Ag_{0.27}Ni_{0.73})_{37}RGO_{63}$ also showed the intimate attachment of Ag and Ni particles (Fig. S5–S7, ESI†). EDS analysis of the samples also confirmed the composition of the composites (Fig. S8 and S9, ESI†).

3.2. Formation mechanism of $(Ag_xNi_{(1-x)})_yRGO_{(100-y)}$ nanocomposites

In this '*in situ*' co-precipitation reduction method the formation of Ni and Ag nanoparticles might occur due to the following reactions:[53–55] When $Ni(NO_3)_2$ was dissolved in ethylene glycol, Ni^{2+} ion formed the coordination complex with glycol (eqn (5)).

$$Ni^{2+} + 3EG \rightarrow [Ni(EG)_3]^{2+} \quad (5)$$

$$[Ni(EG)_3]^{2+} + mN_2H_4 \rightarrow [Ni(N_2H_4)m]^{2+} + 3EG \quad (6)$$

$$[Ni(N_2H_4)m]^{2+} + 2OH^- \rightarrow Ni(OH)_2 + mN_2H_4 \quad (7)$$

$$2Ni(OH)_2 + N_2H_4 \rightarrow 2Ni^0 + N_2 + 4H_2O \quad (8)$$

where EG: ethylene glycol.

When this complex reacted with N_2H_4, the ligand (*i.e.* EG) was replaced by N_2H_4 and formed another complex $[Ni(N_2H_4)_m]^{2+}$ (eqn (6)). $Ni(OH)_2$ was formed when $[Ni(N_2H_4)_m]^{2+}$ was reacted with OH^- (eqn (7)). The formation of nickel hydroxide from hydrazine complex occurred because $Ni(OH)_2$ is more stable than $Ni[(N_2H_4)_m]^{2+}$, so this transformation is thermodynamically feasible.[53] Then, the formation of Ni nanoparticles occurred *via* the reduction of nickel hydroxide by hydrazine (eqn (8)).

Ag nanoparticles were produced *via* the reduction of Ag^+ ions by ethylene glycol and N_2H_4. Ethylene glycol was converted to acetaldehyde after losing one molecule of H_2O (eqn (9)). Then, Ag^+ ions were reduced by acetaldehyde and formed Ag nanoparticles (eqn (10)). Simultaneously, N_2H_4 also reduced Ag^+ and produced Ag nanoparticles (eqn (11)).[56–58]

$$HO–(CH_2)_2–OH \rightarrow CH_3CHO + H_2O \quad (9)$$

$$2Ag^+ + 2CH_3CHO \rightarrow 2Ag^0 + 2H^+ + CH_3COCOCH_3 \quad (10)$$

$$4Ag^+ + N_2H_4 \rightarrow 4Ag^0 + N_2 + 4H^+ \quad (11)$$

In this '*in situ*' co-precipitation reduction technique to synthesize $(Ag_xNi_{(1-x)})_yRGO_{(100-y)}$, hydrazine also reduced GO (particularly its epoxy groups (eqn (12))[1] and converted GO to RGO. Generally, this reduction process initiated from the edges of GO flakes and then moved towards the basal planes.[1] Gao *et al.* have proposed the plausible reaction mechanism for the reduction of the epoxy groups of GO by N_2H_4. The general reaction for this reduction reaction can be presented as eqn (12).[1]

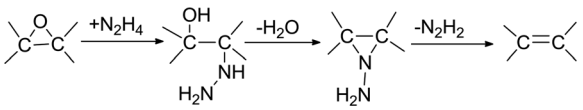

(12)

In this synthesis route, PVP played the role of a capping agent, which prevented the agglomeration of Ag and Ni nanoparticles and restricted their growth. Here, the formation of Ag and Ni nanoparticles and conversion of GO to RGO occurred simultaneously. The unreduced or partially reduced oxygen-containing functional groups of RGO helped to immobilize the Ag and Ni nanoparticles on the surface of nanometer thin RGO sheets. These metal nanoparticles also acted as a spacer between the RGO layers and prevented the agglomeration of RGO sheets.[59,60]

3.3. First-principles calculations of electronic structure

To understand the interfacial interactions between Ag, Ni, and graphene in the synthesized catalysts, we have performed the first-principles calculations based on DFT. The superlattice structures of Ag, Ni, graphene, Ag–Ni interface, and Ag–Ni-graphene before and after full relaxation are presented in Fig. S10 and S11 (ESI†). The lattice parameters obtained for the unit cell of Ag and Ni were 4.08 and 3.52 Å, respectively. These values matched well with the reported values. E. Schiavo *et al.* and F. Cinquini *et al.* have reported the values of lattice parameter of Ag and Ni 4.09 Å (ref. 61 and 62) and 3.52 Å,[63] respectively. In the Ag–Ni superlattice, the binding energy between Ag and Ni was −5.68 eV, which indicated the existence of the interaction between Ag and Ni in the interface. In Ag–Ni-graphene superlattice, the binding energy between Ag–Ni interface and graphene was −3.32 eV, which also indicated the existence of strong interaction between them. The equilibrium interlayer distance between Ag–Ni interface and graphene was 3.29 Å.

The electronic total charge density for the interface between Ag and Ni is shown in Fig. 4d, which clearly shows the orbital overlap between Ag and Ni in the interface. From this plot, it was observed that due to this interaction electron deficient centres were formed on/near the Ni atoms. The higher value of electronegativity of Ag (1.93) than that of Ni (1.91) might be responsible for this. The difference charge density plot of Ag–Ni (Fig. 4f), where the blue color represents the charge depletion and the red color represents the charge accumulation, also indicated the formation of electron deficient center on/near Ni atoms. The charge density distribution plot (Fig. 4e) and the difference charge density plot (Fig. 4g) of Ag–Ni-graphene clearly exhibited the interaction between Ag–Ni, C–Ag, and C–Ni in the interface.

For in-depth understanding of the interactions which exist in the interfaces between Ag–Ni, and Ag–Ni-graphene, their Density of States (DOS), Projected Density of States (PDOS), and band structures were studied (Fig. S12–19, ESI†). Zero band gap of graphene was clearly shown by the band structure of graphene (Fig. S17, ESI†). This plot also showed that the valence bands and the conduction bands are either separated by a gap or overlapped with each other which intersect in two equivalent points, known as Dirac points in the first Brillouin zone.[64,65] The band structures of Ag, Ni, and Ag–Ni-graphene also showed their metallic character (Fig. S12–19, ESI†). In the band structure of Ag–Ni interface the appearance of new bands near the Fermi level compared to Ag and Ni indicated the effect of Ag on the electronic property of Ni. PDOS of Ag–Ni interface (Fig. S15–S16, ESI†) also indicated the strong hybridization between Ni 3d, Ni 4s, Ag 4d and Ag 5s. The PDOS on the d band of Ni, which is positioned between −4 eV to −5 eV below the Fermi level, was found to be enhanced, and the width of d-band was broadened, indicating the hybridization of Ni 3d with Ag 4d states.[66] PDOS of Ag–Ni-graphene (Fig. S18–S19, ESI†) indicated the strong hybridization between C 2p states of graphene and Ni 3d and Ag 4d at valance and conduction band. Due to this hybridization, we can predict that the conductivity of the composite will be increased when graphene will be incorporated in the system. The EIS measurements (Nyquist plot, Fig. S20, ESI†) of the synthesized catalysts supported this by showing the charge transfer resistance (R_{ct}) of $(Ag_{0.27}Ni_{0.73})_{37}RGO_{63}$ (0.144Ω) is much lower than that of RGO (2.073Ω), $Ag_{0.50}Ni_{0.50}$ (0.275Ω), Ni(0.85Ω), and Ag (3.11Ω), indicating the enhanced conductivity of $(Ag_{0.27}Ni_{0.73})_{37}RGO_{63}$. The DFT calculations showed that the

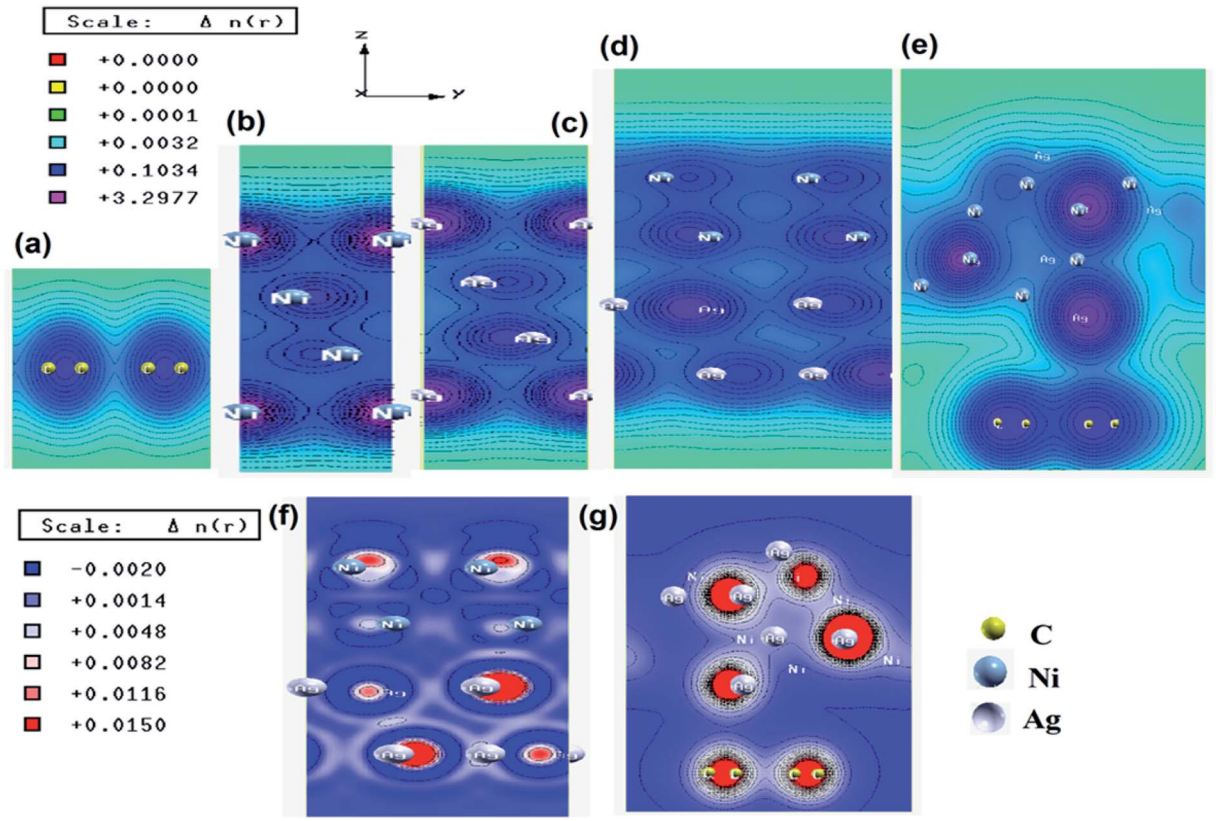

Fig. 4 Electronic total charge density plot of (a) graphene, (b) Ni slab, (c) Ag slab, (d) Ag–Ni interface, (e) Ag–Ni-graphene superlattice, difference charge density plots of (f) Ag–Ni interface, and (g) Ag–Ni-graphene superlattice (where red color represents charge accumulation and blue color represents charge depletion in difference charge density plot).

strong interfacial interaction and orbital level hybridization between Ag, Ni, and graphene in Ag–Ni-graphene superlattice originate the formation of electron deficient Ni centres and enhancement of electrical conductivity in Ag–Ni-graphene. These factors might play important roles in the intermediate formation, and faster charge transfer process during the catalysis reactions. Therefore, we can predict that the synthesized catalyst $(Ag_xNi_{(1-x)})_yRGO_{(100-y)}$ will show better catalytic activity than that of pure Ag, or pure Ni, or Ag–Ni. This prediction agrees well with our experimental results which have been discussed in details in Sections 3.4.

3.4. Catalytic activity of $(Ag_xNi_{(1-x)})_yRGO_{(100-y)}$

3.4.1 Reduction of 4-NP in presence of $NaBH_4$. To evaluate the catalytic activity of the synthesized catalysts, the reduction reaction of 4-nitrophenol (4-NP) to 4-aminophenol (4-AP) in presence of excess $NaBH_4$ in aqueous medium was investigated as a model reaction. To understand the effect of incorporation of RGO and Ag along with Ni in the catalyst composite, first, the catalysis reaction was performed using pure Ni nanoparticles as the catalyst. It has been observed that under this reaction condition, the reaction was completed within 30 min and the time required to initiate the reaction was ~8 min. The $Ni_{40}RGO_{60}$ catalyst, where Ni nanoparticles are dispersed on the surface of RGO nanosheets, exhibited a remarkable increase in catalytic activity. The reaction was completed within 18 min and the time required to initiate the reaction was ~4 min. This result clearly indicated the beneficial effect of RGO. To understand the effect of the incorporation of Ag in the catalyst composition on its catalytic activity, the catalyst was prepared with 5 wt% Ag and 95 wt% Ni ($Ag_{0.05}Ni_{0.95}$). The catalytic activity of this catalyst was found to be better than that of pure Ni particles. In this case, 22 min were required to complete the reaction with ~4 min initiation time. These results clearly demonstrated that the presence of both Ag and RGO enhanced the catalytic activity of the catalyst. To tune the compositions of the catalyst, catalysts having varying wt% of Ag, Ni, and RGO were prepared. The change of reaction completion time and the apparent rate constant (k_{app}) with changing composition of the catalyst are listed in Table 1 and UV-visible spectra are shown in Fig. S21 (ESI†). It has been observed that, the catalyst composed of 3 wt% Ag, 57% Ni, and 40% RGO ($(Ag_{0.05}Ni_{0.95})_{60}RGO_{40}$) exhibited the highest catalytic activity with reaction completion time of 4 min and the reaction started almost instantly soon after the addition of the catalyst which is shown in Fig. 5e. In this case, the k_{app} was 19.6×10^{-3} s^{-1}. This k_{app} value was found to be similar and in some cases superior than the values reported in the literature for the different metal nanoparticle based catalysts (Table S3, ESI†).

The conversion of 4-NP to 4-AP is a six electron transfer reduction reaction. When this reaction is carried out in the presence of metal nanoparticle catalyst and excess $NaBH_4$, it

Table 1 Comparisons of completion time and rate constant of the synthesized catalysts for the reduction of 4-nitrophenol in presence of $NaBH_4$

Composites	Initiation time (min)	Completion time (min)	Apparent rate constant (k_{app}) s^{-1}
Pure Ni	8	30	2.46×10^{-3}
$Ni_{40}RGO_{60}$	4	18	6.66×10^{-3}
Pure Ag	3	8	10.32×10^{-3}
$Ag_{0.05}Ni_{0.95}$	4	22	1.50×10^{-3}
$Ag_{0.15}Ni_{0.85}$	2	14	4.75×10^{-3}
$Ag_{0.25}Ni_{0.75}$	0	7	10.03×10^{-3}
$Ag_{0.27}Ni_{0.73}$	5	15	5.76×10^{-3}
$(Ag_{0.05}Ni_{0.95})_{90}RGO_{10}$	2	15	4.83×10^{-3}
$(Ag_{0.05}Ni_{0.95})_{70}RGO_{30}$	1	7	13.87×10^{-3}
$(Ag_{0.05}Ni_{0.95})_{60}RGO_{40}$	0	4	19.60×10^{-3}
$(Ag_{0.05}Ni_{0.95})_{50}RGO_{50}$	0	8	9.10×10^{-3}
$(Ag_{0.05}Ni_{0.95})_{40}RGO_{60}$	2	10	8.39×10^{-3}
$(Ag_{0.15}Ni_{0.85})_{33.5}RGO_{66.5}$	1	10	7.86×10^{-3}
$(Ag_{0.27}Ni_{0.73})_{37}RGO_{63}$	0	6	10.83×10^{-3}
$(Ag_{0.37}Ni_{0.63})_{40.5}RGO_{59.5}$	1	9	5.10×10^{-3}

proceeds *via* electron transfer mechanism where relaying of electrons occur from BH_4^- (donor) to 4-NP (acceptor). In the aqueous medium generation of hydrogen from BH_4^- occurs *via* the first adsorption of BH_4^- on the surface of catalyst (metal nanoparticles), followed by electron transfer (ET) to the metal nanoparticles.[11,14,15] According to Ding *et al.* the metal nanoparticles play the role of storing electrons after ET from BH_4^-.[41] The H atoms thus generated attack 4-NP and reduce it.[11]

Several factors are responsible for the high catalytic performance of $(Ag_{0.05}Ni_{0.95})_{60}RGO_{40}$ towards this reaction, such as (i) nanosize of the Ag and Ni particles helps to adsorb BH_4^- ions on their surface, (ii) from the DFT study we have observed that, presence of Ag atoms creates electron deficient sites on/near Ni atoms. These electron deficient Ni atoms become more effective to collect electrons from BH_4^- *via* electron transfer process and to generate hydrogen efficiently. Thus the presence of Ag makes the catalysts more efficient towards the reduction of 4-NP in presence of $NaBH_4$, (iii) presence of RGO in the catalyst also helps to enhance its catalytic activity by providing larger surface area. RGO exhibits high adsorption capacity of 4-NP due to π–π stacking interaction.[3,10] Rout *et al.* have reported that due to the strong adsorption of 4-NP onto the surface of RGO, the N=O bond of $-NO_2$ group becomes stretched out (from 1.23 Å to 1.28 Å) and this helps to activate the $-NO_2$ group for the reduction reaction and convert to $-NH_2$ group.[9] (iv) DFT study also showed the existence of hybridization in the orbital level between Ag, Ni, and graphene. Due to these interfacial interactions, the electrical conductivity of the catalyst enhances. (EIS measurements also showed the increase of the conductivity of catalyst due to the presence of RGO Fig. S20, ESI†). This increase of conductivity, as well as the highly conjugated π bonding RGO system facilitates the charge transfer between the catalytically active sites and the reactant molecules (*i.e.* 4-NP). These factors improve the efficiency of the catalyst ($(Ag_{0.05}Ni_{0.95})_{60}RGO_{40}$).

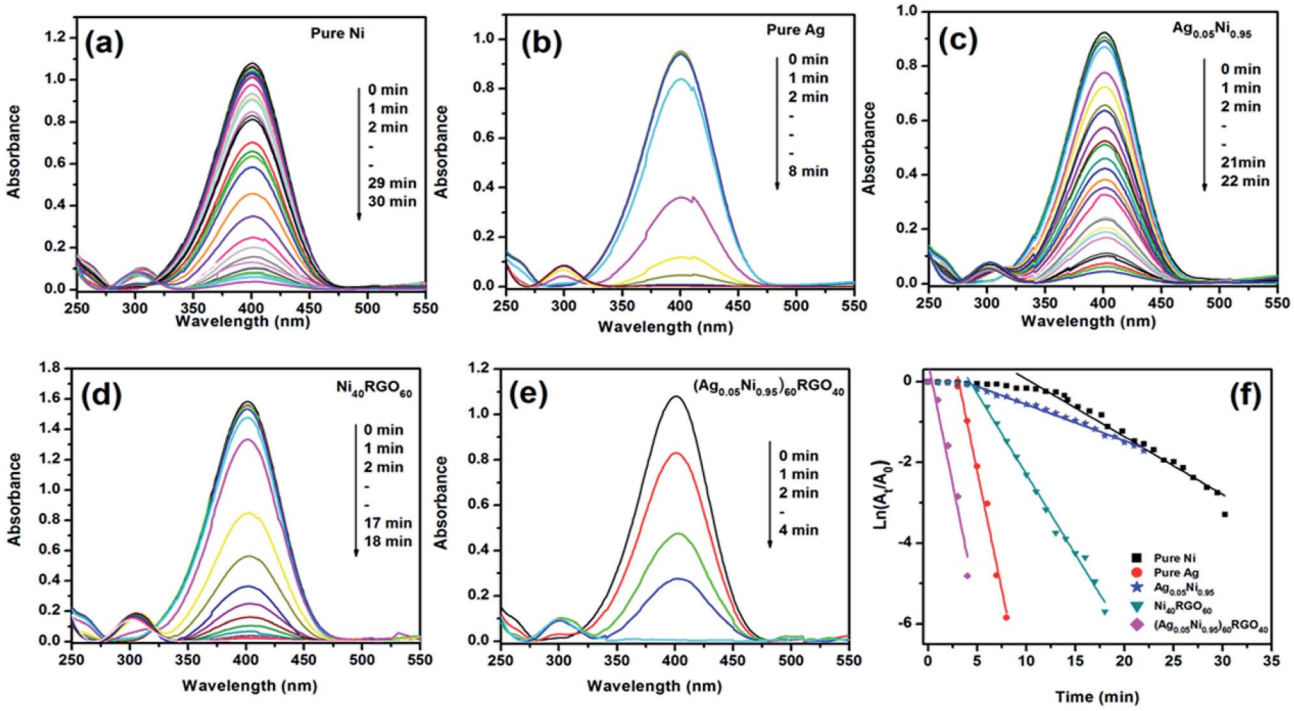

Fig. 5 Time dependent UV-Vis spectral changes of the reaction mixture of 4-NP catalyzed by (a) pure Ni, (b) pure Ag, (c) $Ag_{0.05}Ni_{0.95}$, (d) $Ni_{40}RGO_{60}$, (e) $(Ag_{0.05}Ni_{0.95})_{60}RGO_{40}$, and (f) pseudo first order kinetic plot of 4-NP reduction reaction with pure Ni, Pure Ag, $Ag_{0.05}Ni_{0.95}$, $Ni_{40}RGO_{60}$, and $(Ag_{0.05}Ni_{0.95})_{60}RGO_{40}$.

3.4.2 A3 coupling reaction. We have synthesized different propargylamines to demonstrate the catalytic activity of the synthesized catalysts ($(Ag_xNi_{(1-x)})_yRGO_{(100-y)}$) towards A3 coupling reaction. For this purpose, first the synthesis of *N*,*N*-diethyl-3-phenylprop-2-yn-1-amine was conducted as a model reaction where phenylacetylene, paraformaldehyde, and diethylamine were used as starting materials and acetonitrile was used as the solvent. The reaction can be presented as (13):[17,37]

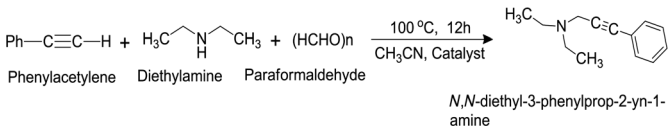

(13)

This reaction was performed in presence of the catalysts with varying compositions. When the reactions were conducted without any catalyst or with pure RGO no product was formed. When pure Ni particle was used as a catalyst, ~71% yield was obtained. Incorporation of Ag nanoparticle in the catalyst resulted in the enhancement of the yield. For example, the yield was increased to ~80% when $Ag_{0.50}Ni_{0.50}$ was the catalyst. To investigate the effect of RGO in the catalyst, the catalysts were prepared by immobilizing Ni nanoparticles on the surface of RGO (*e.g.* $Ni_{10}RGO_{90}$, $Ni_{20}RGO_{80}$, and $Ni_{30}RGO_{70}$ where the amount of RGO was 90, 80 and 70 wt%, respectively). $Ni_{30}RGO_{70}$ showed better catalytic performance (yield ~80%) than that of pure Ni (yield ~71%). As it has been observed that the presence of Ag and RGO with Ni enhanced the yield, now the catalysts were prepared where both Ag and Ni particles were immobilized on the surface of RGO and found to be beneficial in terms of catalytic activity. The % of yield of the product obtained by the catalysts having different compositions are listed in Table S4 (ESI†). It was observed that the catalyst $(Ag_{0.27}Ni_{0.73})_{37}RGO_{63}$ generated the highest yield of ~95%. The % of yields of the product which were obtained at different reaction conditions are listed in Table S5 (ESI†). To demonstrate the applicability of this catalyst for the A3 reaction, several other propargylamines were also synthesized by using different amines and aldehydes. It was observed that reasonably good yield (~80–87%) was obtained and listed in Table 2. The LC-MS, ^{1}H NMR, and FT-IR data of the products are provided in ESI (Spectral data section, Fig. S27–29, ESI†).

The comparison of catalytic activity in terms of % yield of *N*,*N*-diethyl-3-phenylprop-2-yn-1-amine of different reported catalysts with that of $(Ag_{0.27}Ni_{0.73})_{37}RGO_{63}$ is listed in Table S6 (ESI†) and it was observed that the catalytic activity of the synthesized catalyst is comparable with the reported catalysts.[17,18,23,67]

The reaction mechanisms for nanoparticles catalysed A3 coupling reaction, have been proposed by different researchers.[17,68,69] The reaction generally proceeds *via* the activation of C– H bond of the alkyne in the first step by the formation of a metal acetylide intermediate, which is generated by the reaction of alkyne and the metal nanoparticles. In the second step, this metal acetylide reacts with iminium ion (generated '*in situ*' from the reaction of aldehyde and amine) and forms the corresponding propargylamine. The tentative reaction mechanism is shown in Scheme 1.

In this reaction, the electron deficient centres on the Ni, which are generated due to the presence of Ag in the catalyst, helps to coordinate –C≡C– of phenylacetylene with Ni and subsequently formation of Ni-acetylide intermediate more efficiently. Here also, RGO helps to adsorb the reactant molecules on the surface of the catalyst by providing larger surface area and π–π stacking interaction. The enhancement of the conductivity of the catalyst due to the presence of RGO facilitates the charge transfer between catalytically active sites (*i.e.* metal nanoparticles) and reactant molecules. Therefore, the catalysts which contain Ag, Ni, and RGO show superior catalytic activity than pure Ag, or pure Ni, or Ni–Ag, or Ni-RGO.

3.4.3 Epoxidation reaction. To achieve a relatively clean chlorine free reaction condition for the synthesis of styrene oxide, we have investigated the epoxidation reaction of styrene in presence of TBHP with the synthesized catalysts. The reaction can be presented as (14):[15,33]

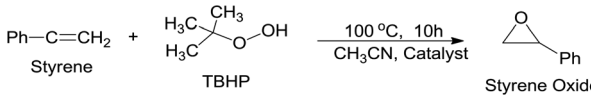

(14)

The reaction was performed in acetonitrile medium by varying the reaction conditions (*e.g.*, temperature, reaction time, styrene : TBHP ratio) and catalyst compositions. When the reaction was performed without catalyst or with pure RGO no desirable product was formed. Table S7 (ESI†) summarizes the effects of catalyst composition on the % of styrene conversion and % of styrene oxide formation. It was observed that the presence of Ag nanoparticle along with Ni particle in the catalyst composite was beneficial for obtaining better styrene conversion and selectivity of styrene oxide formation (Fig. S22, ESI†). The catalytic performance of the catalyst was further improved when Ag and Ni nanoparticles were dispersed on the surface of RGO. When the reaction was performed in the presence of $(Ag_{0.27}Ni_{0.73})_{37}RGO_{63}$ catalyst the highest amount of styrene conversion (96%) with 89% styrene oxide formation selectivity were achieved. The catalytic performance of $(Ag_{0.27}Ni_{0.73})_{37}$-$RGO_{63}$ at different reaction conditions are listed in Table S8 (ESI) (Fig. S23 and S24, ESI†). The catalytic performance of $(Ag_{0.27}Ni_{0.73})_{37}RGO_{63}$ towards the epoxidation reaction of styrene was found to be comparable and in some cases better than that of reported catalysts (Table S9, ESI†).

Several researchers have addressed the epoxidation of styrene on the various catalyst (*e.g.* Ag, Au, Au–$BaTiO_3$, *etc.*).[24,25,30,39,40] The plausible reaction mechanism for the oxidation of styrene to styrene oxide is presented in Scheme 2. In the first step of the reaction, a metal alkyl peroxy intermediate (Intermediate-I) is formed *via* interaction between catalytically active metal nanoparticles and TBHP. When styrene reacts with intermediate I, two type of intermediates (Intermediate II_a and Intermediate II_b) are formed which are isomers of oxametallacyclic species. From Intermediate II_a, epoxide (*i.e.*

Table 2 $(Ag_{0.27}Ni_{0.73})_{37}RGO_{63}$ catalyzed A3 coupling reaction of aldehyde, amine, and phenylacetylene[a]

Entry	Alkyne	Amine	Aldehyde	Product	Yield (%)
1	Ph–C≡C–H	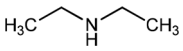	$(HCHO)_n$	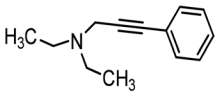	95
2	Ph–C≡C–H	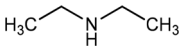	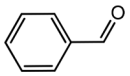	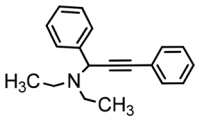	84
3	Ph–C≡C–H		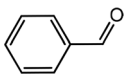	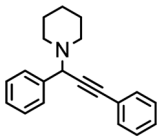	88
4	Ph–C≡C–H		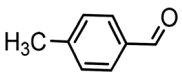	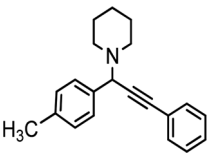	86
5	Ph–C≡C–H		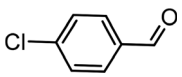	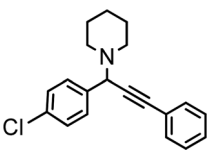	87
6	Ph–C≡C–H		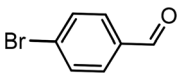	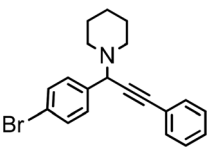	80
7	Ph–C≡C–H		$(HCHO)_n$	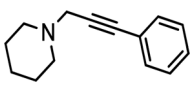	80
8	Ph–C≡C–H	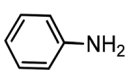	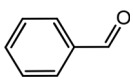	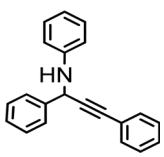	87
9	Ph–C≡C–H	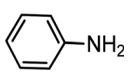	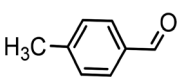	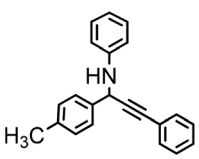	83
10	Ph–C≡C–H	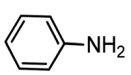	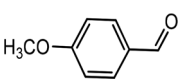	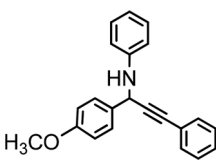	78
11	Ph–C≡C–H	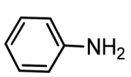	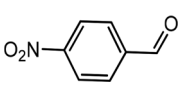	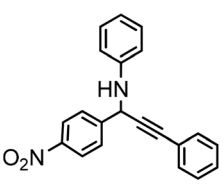	80

[a] Reaction condition: aldehyde (2 mmol), amine (2.4 mmol), phenylacetylene (3 mmol) catalyst $(Ag_{0.27}Ni_{0.73})_{37}RGO_{63}$ 50 mg, acetonitrile 10 ml, reaction temperature 100 °C, reaction time 12 h.

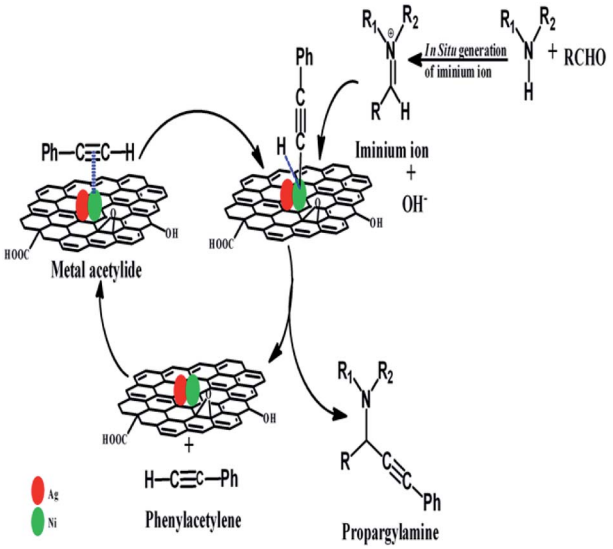

Scheme 1 The tentative reaction mechanism for synthesis of propargylamines *via* A3 coupling reaction.

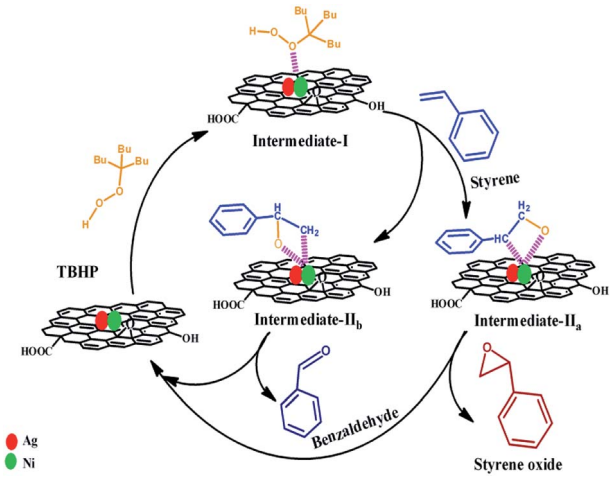

Scheme 2 Plausible reaction mechanism of formation of styrene oxide and benzaldehyde from styrene in presence of TBHP catalyzed by $(Ag_{0.27}Ni_{0.73})_{37}RGO_{63}$.

styrene oxide) is formed *via* sharpless mechanism where the transfer of oxygen occurs to the olefinic bond. On the other hand benzaldehyde forms as a byproduct from Intermediate II_b *via* breakage of the C–C bond.[24]

In the synthesized catalyst $(Ag_xNi_{(1-x)})_yRGO_{(100-y)}$ presence of electron deficient Ni centres helps in the formation of Intermediates II_a and II_b from Intermediate I *via* formation of coordination complexes with metal nanoparticles. Moreover, the presence of RGO helps to adsorb styrene molecule on the surface of the catalyst by π–π interaction. Due to these factors, the catalyst containing Ag, Ni, and RGO showed better catalytic activity than pure Ni, pure Ag, and $Ag_{0.50}Ni_{0.50}$.

3.4.4 Click reaction. We have also performed the synthesis of 1,4-disubstituted 1,2,3-triazoles by 'Click reaction' in the presence of the synthesized catalysts using styrene oxide, phenylacetylene, and sodium azide as a model substrate. The reaction can be presented as (15):[10,34]

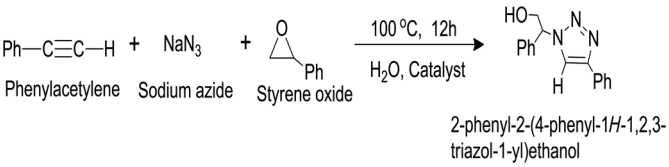

(15)

First, the reaction was performed without any catalyst or with pure RGO and no product was obtained. Then the reactions were carried out in presence of the synthesized catalysts, which are composed of varying amount of Ni, Ag, and RGO. When pure Ni and pure Ag nanoparticles were used as a catalyst, the yield was ~50% and ~48%, respectively. When $Ag_{0.50}Ni_{0.50}$ was used as catalyst the product yield was increased to ~62%, which clearly indicated that the presence of Ag positively influences the catalytic activity property of the catalyst. It has also been observed that, when Ni nanoparticle was dispersed on the surface of RGO, the efficiency of the catalyst was also increased. For example, when $Ni_{30}RGO_{70}$ was used as catalyst the yield was ~66% which is higher than that of pure Ni-catalyzed reaction. This enhancement of the catalytic activity might be due to the following reasons (i) dispersion of Ni particles on the RGO surface prevents the agglomeration of nanoparticles. Therefore, the reactant molecules get more access to the catalytically active sites, (ii) the reactant molecules (*e.g.* styrene oxide, phenylacetylene) are adsorbed more on the surface of the RGO containing catalysts, because of the π–π interaction between RGO sheets and phenyl group of the reactant molecules, (iii) the high conductivity of RGO facilitates the electron transfer process during the reaction.

Table 3 Synthesis of 2-phenyl-2-(4-phenyl-1*H*-1,2,3-triazol-1-yl) ethanol with different synthesized catalyst[a]

Catalyst	Yield (%)
Pure Ni	55
Pure Ag	53
$Ni_{10}RGO_{90}$	26
$Ni_{20}RGO_{80}$	66
$Ni_{30}RGO_{70}$	66
$Ag_{0.50}Ni_{0.50}$	62
$(Ag_{0.15}Ni_{0.85})_{33.5}RGO_{66.5}$	89
$(Ag_{0.27}Ni_{0.73})_{37}RGO_{63}$	91
$(Ag_{0.37}Ni_{0.63})_{40.5}RGO_{59.5}$	90
$(Ag_{0.45}Ni_{0.55})_{44}RGO_{56}$	92

[a] Reaction condition: styrene oxide (1 mmol 0.115 ml), phenylacetylene (1 mmol 0.110 ml) sodium azide (1.5 mmol 97.5 mg), water (3 ml), reaction time 12h, reaction temperature = 100 °C, catalyst dose = 25 mg.

As it has been observed that the presence of Ag and RGO helped in the enhancement of the catalytic activity of Ni, we have tested the catalytic activity of the catalyst, containing varying amount of Ag, Ni, and RGO. The change in % of product

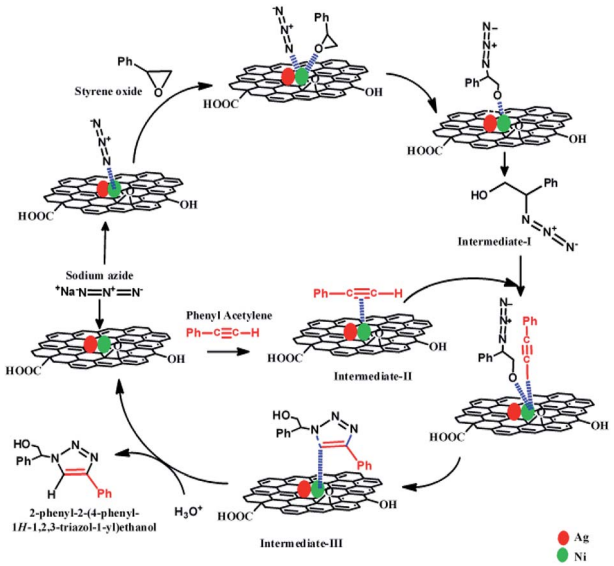

Scheme 3 The tentative reaction mechanism involved for synthesis of 2-phenyl-2-(4-phenyl-1*H*-1,2,3-triazol-1-yl)ethanol *via* Click reaction catalyzed by $(Ag_{0.27}Ni_{0.73})_{37}RGO_{63}$ catalyst.

yield with the variation of the composition of the synthesized catalyst is listed in Table 3. It has been observed that the catalyst containing 10 wt% Ag, 27% Ni, and 63 wt% RGO (*i.e.* $(Ag_{0.27}Ni_{0.73})_{37}RGO_{63}$) showed the highest catalytic activity with ~91% yield. The performance of this catalyst for this reaction was compared with the reported catalysts (Table S10, ESI†) and found to be comparable and in some cases superior to some of the reported results. We have also performed the Click reaction by replacing styrene oxide with cyclohexane oxide (and epichlorohydrine) and found the % of the yield of the corresponding products are ~88% and ~67%.

The tentative reaction mechanism for this Click reaction was proposed by several researchers[10,32,33,35] and shown in Scheme 3. In this reaction, the metal nanoparticles play the role of a catalytically active site and act as a bifunctional catalyst which combines one pot ring opening of epoxy and 1,3-dipolar cyclo addition.[10,32] Initially, catalytically active metal azide is formed which helps to activate epoxide and facilitates the delivery of azide ion during the ring opening of epoxide. Thus, the organoazide intermediate (Intermediate-I) is formed from epoxy and azide. During the same time, another intermediate, metal-acetylide complex (Intermediate-II) forms *via* π complexation between the metal nanoparticle and phenylacetylene. Then coordination of organoazide (Intermediate-I) with the metal centre of metal acetylide (Intermediate II) occurs which enhances the nucleophilicity of –C≡C–. Then 1,3 dipolar cyclo addition reaction results in the formation of the new C–N bond between the nucleophilic β-carbon atom of the acetylide and the terminal electrophilic nitrogen atom of the azide (Intermediate-III).[10,32] After protonation, intermediate-III yields the β-hydroxy-1,2,3-triazole. In this reaction pathway formation of metal azide *via* interaction of metal nanoparticles and N_3^-, and formation of the metal-acetylide complex (which forms *via* π complexation between the metal nanoparticle and phenylacetylene) play critical roles. As the DFT study showed that the presence of Ag causes the formation of electron deficient centres near/on Ni atoms, the formation of metal azide and metal-acetylide occurs efficiently with these electron deficient Ni centres. Moreover, the presence of RGO in the synthesized catalyst also helps to absorb the reactant materials (*e.g.* phenylacetylene, styrene oxide) on the surface of the catalyst. These factors are

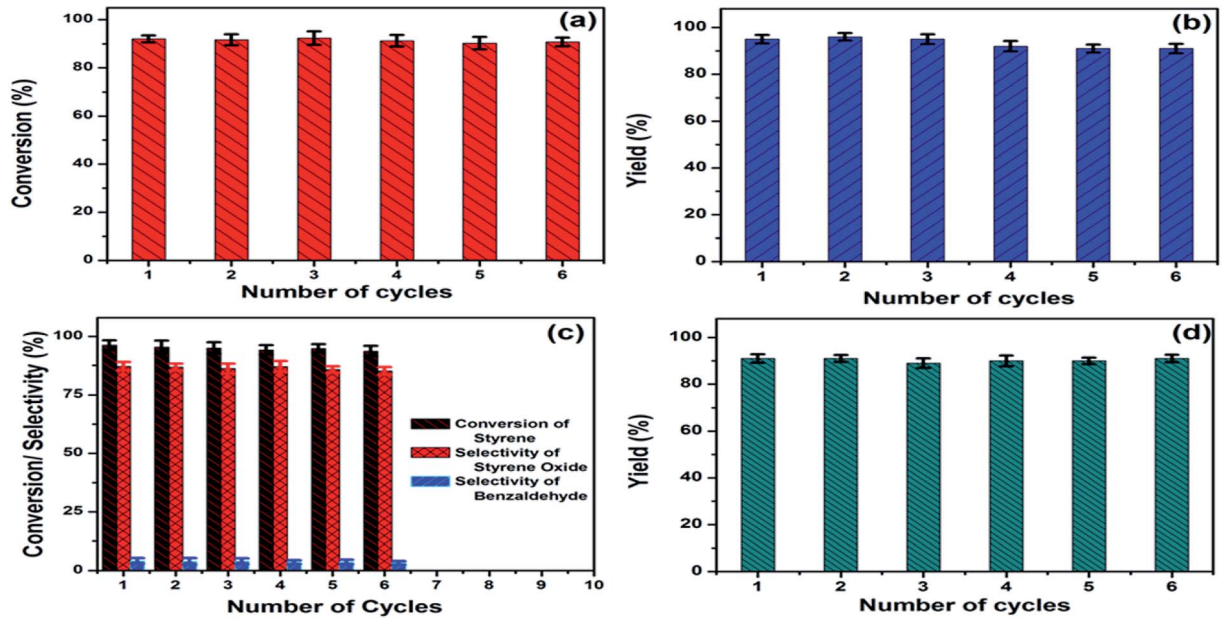

Fig. 6 Reusability of (a) $(Ag_{0.05}Ni_{0.95})_{60}RGO_{40}$ catalyst for the reduction of 4-NP, and $(Ag_{0.27}Ni_{0.73})_{37}RGO_{63}$ catalyst for (b) the synthesis of *N*,*N*-diethyl-3-phenylprop-2-yn-1-amine *via* A3 coupling reaction, (c) the epoxidation reaction of styrene to styrene oxide, and (d) the synthesis of 2-phenyl-2-(4-phenyl-1*H*-1,2,3-triazole-1-yl)ethanol *via* Click reaction.

responsible for the superior catalytic activity of $(Ag_xNi_{(1-x)})RGO_{(100-x)}$ than pure Ag, Ni, or $Ag_{0.50}Ni_{0.50}$.

The details of the spectral analysis of products, which were formed in the A3 coupling reaction, epoxidation reaction of styrene and Click reaction, are provided in ESI (Spectra data section, Fig. S25–S29, ESI†).

3.5. Reusability

The presence of Ni nanoparticle introduced the magnetic character in $(Ag_xNi_{(1-x)})_yRGO_{(100-y)}$ nanocatalyst. Using VSM the saturation magnetization (M_s) and coercivity (H_c) values of the catalysts were determined. For example, M_s and H_c values of $(Ag_{0.27}Ni_{0.73})_{37}RGO_{63}$, were 9.81 emu g^{-1} and 146.5 Oe, respectively (Fig. S30, ESI†). The magnetic character of this catalyst allowed its easy magnetic separation from the reaction mixture. After completion of all the reactions, the catalyst was separated from the reaction mixture by applying a magnet externally (Fig. S31, ESI†) and then washed with distilled water for several times and dried in a vacuum oven at 60 °C for 12 h. The recovered catalyst was used in the next cycle of the catalysis reactions. No significant loss of activity was observed up to 6^{th} reuse for all four reactions and shown in Fig. 6. XRD patterns and FESEM micrograph of the reused catalyst also confirmed that the crystal structure and morphology of the catalyst remained same after 6^{th} catalysis cycle (Fig. S32, ESI†). These results thus clearly demonstrated the structural robustness of the catalyst.

4. Conclusion

Here, we have reported a simple '*in situ*' co-precipitation reduction technique for the preparation of nanocatalyst containing Ag, Ni, and RGO $(Ag_xNi_{(1-x)})_yRGO_{(100-y)}$. In this catalyst Ag and Ni particles were immobilized on the surface of the nanometer thin RGO sheets. Here, RGO provided a highly conductive support to the catalytically active Ni and Ag nanoparticles. DFT studies were performed to obtain the electronic structure and electronic properties of Ag–Ni-graphene. This study helps us to understand the interfacial interactions and orbital level hybridizations which exist in the interfaces between Ag, Ni, and RGO. These interfacial interactions create electron deficient centres near/on the Ni atoms and also enhance the conductivity of the catalyst. The synergistic effect, which arises from the coexistence of Ag, Ni, and RGO in the catalyst, positively influences the catalytic activity of the synthesized catalysts.

Here, it has been demonstrated that combination of Ag, Ni, and RGO in the composition of the catalyst caused significant enhancement of the catalytic activity compared to pure Ag and Ni nanoparticles towards four important reactions (i) reduction of 4-nitrophenol (4-NP) in the presence of $NaBH_4$, (ii) A3 coupling reaction for the synthesis of propargylamines, (iii) epoxidation of styrene, and (iv) 'Click reaction' for the synthesis of 1,2,3-triazole derivatives in aqueous medium. $(Ag_{0.05}Ni_{0.95})_{60}RGO_{40}$ exhibited highest catalytic activity towards the reduction of 4-nitrophenol with k_{app} 19.6 1910^{-3} s^{-1}. In case of the A3 coupling reaction, $(Ag_{0.27}Ni_{0.73})_{37}RGO_{63}$ catalyzed reaction produced *N*,*N*-diethyl-3-phenylprop-2-yn-1-amine with ~95% yield. This same catalyst showed ~96% styrene conversion with ~89% styrene oxide formation selectivity for epoxidation of styrene reaction, and ~91% yield for the synthesis of 2-phenyl-2-(4-phenyl-1*H*-1,2,3-triazol-1-yl)ethanol *via* Click reaction. The catalyst also demonstrated its easy magnetic recovery from the reaction mixture after completion of the reactions. The recovered catalysts also exhibited a very good reusability.

To the best of our knowledge, this is the first time a catalyst having composition $(Ag_xNi_{(1-x)})_yRGO_{(100-y)}$ which showed the versatile catalytic activity towards the aforesaid reactions with high efficiency and also the investigations on the electronic structures of this catalyst by DFT calculations have been reported. The easy synthetic methodology high catalytic performance with very good reusability and easy magnetic recovery make the synthesize catalyst an attractive catalyst.

Conflicts of interest

There are no conflicts to declare.

Acknowledgements

Dr N. N. Ghosh gratefully acknowledges DRDO Jodhpur for VSM analysis. Dr Ghosh is thankful to the Central Sophisticated Instrumentation Facility (CSIF) of BITS Pilani K. K. Birla Goa campus for providing the FESEM and LC-MS facility.

Notes and references

1 X. Gao, J. Jang and S. Nagase, *J. Phys. Chem. C*, 2009, **114**, 832.
2 M. Hu, Z. Yao and X. Wang, *Ind. Eng. Chem. Res.*, 2017, **56**, 3477.
3 D. Moitra, B. Ghosh, M. Chandel, R. Jani, M. Patra, S. Vadera and N. Ghosh, *RSC Adv.*, 2016, **6**, 14090.
4 D. Moitra, M. Chandel, B. K. Ghosh, R. K. Jani, M. K. Patra, S. R. Vadera and N. N. Ghosh, *RSC Adv.*, 2016, **6**, 76759.
5 D. Moitra, C. Anand, B. K. Ghosh, M. Chandel and N. N. Ghosh, *ACS Appl. Energy Mater.*, 2018, **1**, 464.
6 X. Fan, G. Zhang and F. Zhang, *Chem. Soc. Rev.*, 2015, **44**, 3023.
7 O. C. Compton and S. T. Nguyen, *Small*, 2010, **6**, 711.
8 K. Hareesh, R. Joshi, D. Sunitha, V. Bhoraskar and S. Dhole, *Appl. Surf. Sci.*, 2016, **389**, 1050.
9 L. Rout, A. Kumar, R. S. Dhaka, G. N. Reddy, S. Giri and P. Dash, *Appl. Catal., A*, 2017, **538**, 107.
10 D. Moitra, B. K. Ghosh, M. Chandel and N. N. Ghosh, *RSC Adv.*, 2016, **6**, 97941.
11 T. Aditya, A. Pal and T. Pal, *Chem. Commun.*, 2015, **51**, 9410.
12 M. Chandel, D. Moitra, P. Makkar, H. Sinha, H. S. Hora and N. N. Ghosh, *RSC Adv.*, 2018, **8**, 27725.
13 H. Hu, J. H. Xin, H. Hu, X. Wang, D. Miao and Y. Liu, *J. Mater. Chem. A*, 2015, **3**, 11157.
14 B. Naik, S. Hazra, V. S. Prasad and N. N. Ghosh, *Catal. Commun.*, 2011, **12**, 1104.

15 B. K. Ghosh, D. Moitra, M. Chandel, H. Lulla and N. N. Ghosh, *Mater. Res. Bull.*, 2017, **94**, 361.
16 Y.-g. Wu, M. Wen, Q.-s. Wu and H. Fang, *J. Phys. Chem. C*, 2014, **118**, 6307.
17 T. K. Saha and R. Das, *ChemistrySelect*, 2018, **3**, 147.
18 N. Hussain and M. R. Das, *New J. Chem.*, 2017, **41**, 12756.
19 S. Frindy, A. El Kadib, M. Lahcini, A. Primo and H. García, *Catal. Sci. Technol.*, 2016, **6**, 4306.
20 A. M. Munshi, M. Shi, S. P. Thomas, M. Saunders, M. A. Spackman, K. S. Iyer and N. M. Smith, *Dalton Trans.*, 2017, **46**, 5133.
21 X. Zhang and A. Corma, *Angew. Chem.*, 2008, **120**, 4430.
22 K. Namitharan and K. Pitchumani, *Eur. J. Org. Chem.*, 2010, **3**, 411.
23 N. Salam, A. Sinha, A. S. Roy, P. Mondal, N. R. Jana and S. M. Islam, *RSC Adv.*, 2014, **4**, 10001.
24 D. Nepak and D. Srinivas, *Appl. Catal., A*, 2016, **523**, 61.
25 Q. Wang, C. Li, J. Bai, W. Sun and J. Wang, *J. Inorg. Organomet. Polym. Mater.*, 2016, **26**, 488.
26 V. R. Choudhary, R. Jha and P. Jana, *Catal. Commun.*, 2008, **10**, 205.
27 D.-H. Zhang, H.-B. Li, G.-D. Li and J.-S. Chen, *Dalton Trans.*, 2009, **47**, 10527.
28 A. Wang and H. Jing, *Dalton Trans.*, 2014, **43**, 1011.
29 B. Sakthivel, D. S. R. Josephine, K. Sethuraman and A. Dhakshinamoorthy, *Catal. Commun.*, 2018, **108**, 41.
30 A. S. Sharma and H. Kaur, *Appl. Catal., A*, 2017, **546**, 136.
31 A. N. Prasad, B. Thirupathi, G. Raju, R. Srinivas and B. M. Reddy, *Catal. Sci. Technol.*, 2012, **2**, 1264.
32 H. Naeimi and Z. Ansarian, *Appl. Organomet. Chem.*, 2017, **31**, e3796.
33 B. K. Ghosh, D. Moitra, M. Chandel, M. K. Patra, S. R. Vadera and N. N. Ghosh, *Catal. Lett.*, 2017, **147**, 1061.
34 B. K. Ghosh, S. Hazra and N. N. Ghosh, *Catal. Commun.*, 2016, **80**, 44.
35 C. Wang, D. Ikhlef, S. Kahlal, J.-Y. Saillard and D. Astruc, *Coord. Chem. Rev.*, 2016, **316**, 1.
36 B. A. Kumar, K. H. V. Reddy, B. Madhav, K. Ramesh and Y. Nageswar, *Tetrahedron Lett.*, 2012, **53**, 4595.
37 X. Huo, J. Liu, B. Wang, H. Zhang, Z. Yang, X. She and P. Xi, *J. Mater. Chem. A*, 2013, **1**, 651.
38 R. N. Baig and R. S. Varma, *Chem. Commun.*, 2013, **49**, 752.
39 D.-H. Zhang, G.-D. Li, J.-X. Li and J.-S. Chen, *Chem. Commun.*, 2008, **29**, 3414.
40 X. Wang, Z. Liang, F. Zhang, L. Yang and S. Xu, *J. Mater. Sci.*, 2013, **48**, 5899.
41 M. Gopiraman, D. Deng, S. Saravanamoorthy, I.-M. Chung and I. S. Kim, *RSC Adv.*, 2018, **8**, 3014.
42 W. Hummers and R. Offeman, *J. Am. Chem. Soc.*, 1958, **80**, 1339.
43 P. Giannozzi, S. Baroni, N. Bonini, M. Calandra, R. Car, C. Cavazzoni, D. Ceresoli, G. L. Chiarotti, M. Cococcioni and I. Dabo, *J. Phys.: Condens. Matter*, 2009, **21**, 395502.
44 I. Solovyev, P. Dederichs and V. Anisimov, *Phys. Rev. B: Condens. Matter Mater. Phys.*, 1994, **50**, 16861.
45 J. P. Perdew, K. Burke and M. Ernzerhof, *Phys. Rev. Lett.*, 1996, **77**, 3865.
46 S. Grimme, *J. Comput. Chem.*, 2004, **25**, 1463.
47 S. Grimme, *J. Comput. Chem.*, 2006, **27**, 1787.
48 Quantum ESPRESSO, Files: C.pbe-n-rrkjus_psl.1.0.0.UPF, Ag.pbe-n-rrkjus_psl.1.0.0.UPF, and Ni.pbe-n-rrkjus_psl.1.0.0.UPF, https://www.quantum-espresso.org/pseudopotentials, (accessed February 2018).
49 H. J. Monkhorst and J. D. Pack, *Phys. Rev. B: Condens. Matter Mater. Phys.*, 1976, **13**, 5188.
50 M. Methfessel and A. Paxton, *Phys. Rev. B: Condens. Matter Mater. Phys.*, 1989, **40**, 3616.
51 N. Marzari, D. Vanderbilt, A. De Vita and M. Payne, *Phys. Rev. Lett.*, 1999, **82**, 3296.
52 M. Zong, Y. Huang, Y. Zhao, X. Sun, C. Qu, D. Luo and J. Zheng, *RSC Adv.*, 2013, **3**, 23638.
53 Z. G. Wu, M. Munoz and O. Montero, *Adv. Powder Technol.*, 2010, **21**, 165.
54 D. Knetsch and W. Groeneveld, *Inorg. Chim. Acta*, 1973, **7**, 81.
55 S.-H. Wu and D.-H. Chen, *J. Colloid Interface Sci.*, 2003, **259**, 282.
56 T. Zhao, R. Sun, S. Yu, Z. Zhang, L. Zhou, H. Huang and R. Du, *Colloids Surf., A*, 2010, **366**, 197.
57 U. Nickel, A. zu Castell, K. Pöppl and S. Schneider, *Langmuir*, 2000, **16**, 9087.
58 J. H. Byeon and Y.-W. Kim, *Ultrason. Sonochem.*, 2012, **19**, 209.
59 R. Dhanda and M. Kidwai, *J. Mater. Chem. A*, 2015, **3**, 19563.
60 L. Liu, J. Xue, X. Shan, G. He, X. Wang and H. Chen, *Catal. Commun.*, 2016, **75**, 13.
61 E. Schiavo, A. B. Muñoz-García, V. Barone, A. Vittadini, M. Casarin, D. Forrer and M. Pavone, *Chem. Phys. Lett.*, 2018, **693**, 28.
62 R. Wyckoff, *Crystal structures*, 1963, vol. 1, p. 85.
63 F. Cinquini, F. Delbecq and P. Sautet, *Phys. Chem. Chem. Phys.*, 2009, **11**, 11546.
64 P. Khomyakov, G. Giovannetti, P. Rusu, G. v. Brocks, J. Van den Brink and P. J. Kelly, *Phys. Rev. B: Condens. Matter Mater. Phys.*, 2009, **79**, 195425.
65 C. Gong, G. Lee, B. Shan, E. M. Vogel, R. M. Wallace and K. Cho, *J. Appl. Phys.*, 2010, **108**, 123711.
66 Y.-A. Zhu, D. Chen, X.-G. Zhou, P.-O. Åstrand and W.-K. Yuan, *Surf. Sci.*, 2010, **604**, 186.
67 C. Wei, Z. Li and C.-J. Li, *Synlett*, 2004, **09**, 1472.
68 G.-P. Yong, D. Tian, H.-W. Tong and S.-M. Liu, *J. Mol. Catal. A: Chem.*, 2010, **323**, 40.
69 W. Yan, R. Wang, Z. Xu, J. Xu, L. Lin, Z. Shen and Y. Zhou, *J. Mol. Catal. A: Chem.*, 2006, **255**, 81.